

# The all-seeing eye of resonant Auger electron spectroscopy: a study on aqueous KCl

Tsveta Miteva,<sup>†</sup> Nikolai Kryzhevoi,<sup>‡</sup> Nicolas Sisourat,<sup>†</sup> Christophe Nicolas,<sup>¶</sup>  
Wandared Pokapanich,<sup>§</sup> Th. Saisopa,<sup>||</sup> P. Songsiriritthigul,<sup>||</sup> Y. Rattanachai,<sup>⊥</sup>  
Andreas Dreuw,<sup>#</sup> Jan Wenzel,<sup>#</sup> Jérôme Palaudoux,<sup>†</sup> Gunnar Öhrwall,<sup>†</sup> Ralph  
Püttner,<sup>@</sup> Lorenz S. Cederbaum,<sup>‡</sup> Jean-Pascal Rueff,<sup>†</sup> and Denis Céolin<sup>\*,¶</sup>

<sup>†</sup>*Sorbonne Université, CNRS, Laboratoire de Chimie Physique Matière et Rayonnement,  
UMR 7614, F-75005 Paris, France*

<sup>‡</sup>*Theoretische Chemie, Physikalisch-Chemisches Institut, Universität Heidelberg, Im  
Neuenheimer Feld 229, D-69120 Heidelberg, Germany*

<sup>¶</sup>*Synchrotron SOLEIL, l'Orme des Merisiers, Saint-Aubin, F-91192 Gif-sur-Yvette Cedex,  
France*

<sup>§</sup>*Faculty of Science, Nakhon Phanom University, Nakhon Phanom 48000 Thailand*

<sup>||</sup>*NANOTEC-SUT Center of Excellence on Advanced Functional Nanomaterials and School  
of Physics, Suranaree University of Technology, Nakhon Ratchasima 30000, Thailand*

<sup>⊥</sup>*Department of Applied Physics, Faculty of Sciences and Liberal Arts, Rajamangala  
University of Technology Isan, Nakhon Ratchasima 30000, Thailand*

<sup>#</sup>*Interdisciplinary Center for Scientific Computing, Ruprecht-Karls University, Im  
Neuenheimer Feld 205A, D-69120 Heidelberg, Germany*

<sup>@</sup>*Fachbereich Physik, Freie Universität Berlin, Arnimallee 14, D-14195, Berlin, Germany*

E-mail: denis.ceolin@synchrotron-soleil.fr

## Abstract

X-ray absorption and Auger electron spectroscopies are powerful tools to probe the electronic structure and immediate surroundings of ions in a solution. In this work we use a combination of these methods to study the electronic structure and decay in aqueous KCl at the K-edges of  $\text{K}^+$  and  $\text{Cl}^-$ . Although the two ions are isoelectronic, their Auger electron spectra as a function of the photon energy exhibit notably different features. To explain these differences, we carried out *ab initio* calculations of both the core excited states and the final Auger states of  $\text{K}^+$ ,  $\text{Cl}^-$  and their microsolvated clusters. Our calculations show that the energy order of the 3d and 4p orbitals is inverted in  $\text{K}^+$  with respect to  $\text{Cl}^-$ . The reverse orbital order in the two ions is reflected in both the ordering of the core excited states and in the final states populated in the resonant Auger decay. The energetic proximity of the 3d and 4p virtual states in the bare  $\text{K}^+$  ion leads to their mixing in the presence of the solvent, and to the population of the dipole forbidden  $1s \rightarrow 3d$  state upon K-shell excitation in an aqueous solution. The resonant Auger decay of this state results in a separate feature in the Auger electron spectrum of  $\text{K}^+$  which is absent in the spectrum of  $\text{Cl}^-$ . The results of this work represent a pioneering study of the decay processes initiated by photoabsorption in the tender x-ray regime close to threshold in liquids and are thus of importance in unveiling the mechanisms of radiation damage in biologically relevant systems.

## Introduction

X-ray absorption and Auger electron spectroscopies are powerful tools to study the electronic structure and the nearest environment of atoms and molecules in gas, liquid and solid phase. Understanding how atoms or molecules respond to irradiation with x-rays gives insight into the structure of solutions (see Ref.<sup>1</sup> and references therein), and the mechanism of radiation damage<sup>2-4</sup>. Upon absorption of an x-ray photon, core excited or core ionized states of a specific atom are populated depending on the photon energy. The relaxation of these highly energetic states involves an ultrafast cascade of intraatomic processes, such as radiative and

Auger decays. Furthermore, if the initially excited or ionized species is embedded in an environment, interatomic processes such as charge and energy transfer<sup>4-8</sup> are possible.

The course of a decay cascade depends on the character of the initially populated states. This has been well understood in atoms and molecules in gas phase<sup>9-16</sup>. In the case of a core ionized state, the Auger decay process, designated as normal Auger decay (see Fig. 1), leads to the population of doubly ionized final states localized on the initially ionized unit<sup>9-12</sup>. Auger processes in rare gas clusters have been also investigated (refs). The normal Auger decay process in clusters proceeds similarly to that in atoms or molecules. However, in the case of a core excited state, the resonant Auger process competes with the process of delocalization of the excited electron in clusters. If the initially core excited electron delocalizes within the lifetime of the core hole, then normal instead of resonant Auger decay is observed<sup>17</sup>.

In a solution, the electronic decay processes initiated by x-ray photoabsorption are different compared to those in rare gas clusters due to the shorter distances and stronger interatomic interactions. In particular, the solvent molecules have two effects – first, they strongly affect the excited<sup>18</sup> or ionized states of the ion and second, they can participate in the decay processes, leading to the population of charge-separated final states, and ionization of the surrounding environment<sup>4-6,8</sup>. Moreover, the process of delocalization of the initially excited electron also occurs in aqueous solutions<sup>19,20</sup>. In the case of pure water, the rate of delocalization of the O1s excited electron takes place on a femtosecond to sub-femtosecond time scale depending on the photon energy, thus being commensurate with the lifetime of the O1s core hole which is 6 fs<sup>19</sup>. The O K-edge is located in the soft x-ray range of photon energies. Going higher in photon energy, in the tender and hard x-ray regimes, the lifetimes of the core ionized or core excited states become even shorter, on the order of 1 fs. And thus, it is even more imperative to reveal whether the delocalization of the core excited electron occurs within the lifetime of the core hole.

The aim of this work is to elucidate the nature of the states populated upon x-ray

irradiation of solvated ions in the tender x-ray regime, and furthermore, to understand whether the process of delocalization influences the resonant Auger decay. To this end, we used Auger electron spectroscopy together with x-ray absorption spectroscopy in the tender x-ray regime to study aqueous potassium chloride at the K-edges of both  $\text{K}^+$  and  $\text{Cl}^-$ . In particular, we demonstrate experimentally that at photon energies below the K-edges of the two ions, localized core excited states are populated. These states undergo resonant Auger decay within less than 1 fs. In both ions, there is a competition between resonant Auger decay and delocalization of the excited electron. Using the core-hole clock method we show that in  $\text{K}^+$  delocalization at the pre-edge is weak, whereas in the case of  $\text{Cl}^-$ , due to the energetic proximity of the core excited state to the K-edge, the rate of delocalization is of the same order as that of the resonant Auger process. Moreover, we observe that although the  $\text{K}^+$  and  $\text{Cl}^-$  ions are isoelectronic, they have different fingerprints in the resonant Auger spectra. With the aid of high-level *ab initio* calculations of the initial and final states of the resonant Auger process of both the bare ions and their microsolvated clusters, we demonstrate that these differences result from different electronic structures of the two ions, thus confirming that the combination of XAS and AES techniques is a sensitive probe of the electronic structure of solutions.

## Methods

### Experimental

For the present experiment we used the newly operational microjet setup that was specifically designed for the HAXPES station of the GALAXIES beamline<sup>21,22</sup>. A differentially-pumped tube in which the microjet head is inserted, is mounted on a 3-axes manipulator in front of the spectrometer lens. Two holes of 2 mm diameter allow the photons to go in and out. At the end of the tube and in front of the lens, a 500  $\mu\text{m}$  diameter hole skimmer allows the electrons created at the interaction point to go in the direction of the spectrometer. The microjet

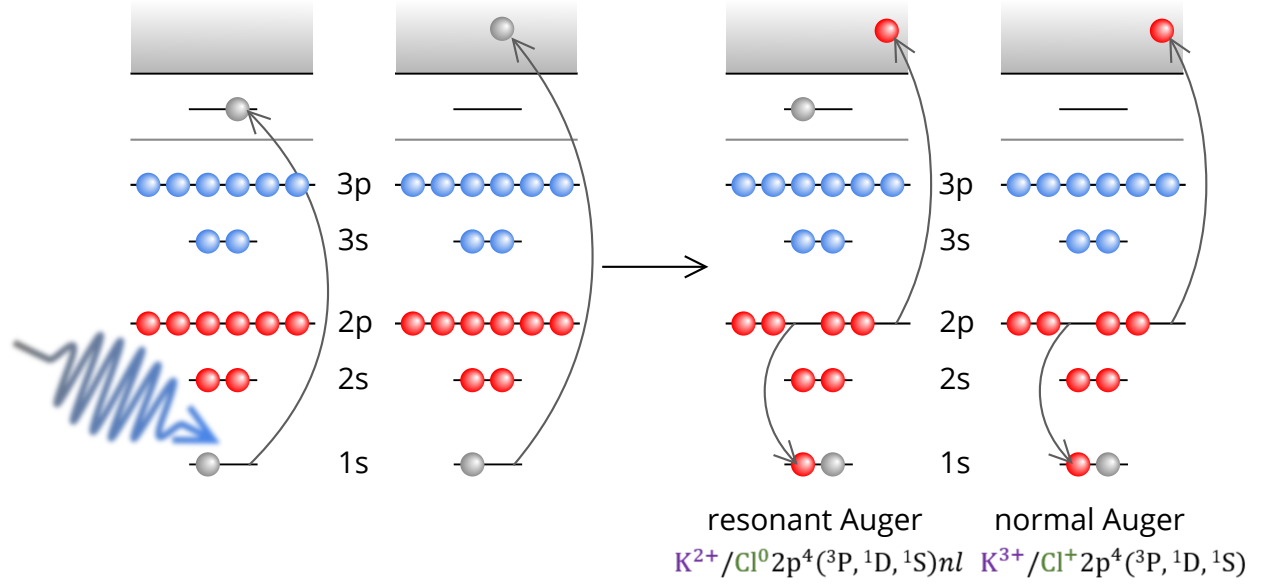


Figure 1: Schematic representation of the normal and resonant Auger processes of the iso-electronic  $K^+$  and  $Cl^-$  ions. The charges of the final Auger states in the two ions are also shown.

head is mostly composed of a  $30\ \mu\text{m}$  diameter vertical glass capillary facing a temperature-controlled catcher in CuBe having a  $300\ \mu\text{m}$  hole, and a camera. Piezo motors allow their precise alignment relative to each other and to the photon beam. The catcher is placed at a distance of about 5 mm from the capillary and is permanently pumped in order to extract the liquid. For the present experiment, a 0.5M KCl aqueous solution is injected in the capillary by a high performance liquid chromatography (HPLC) pump with a constant flux of 1.6 ml/min. The alignment of the setup is performed on a salted aqueous solution by measuring the O1s XPS peak intensity and by optimizing the liquid phase vs gas phase ratio. The pressure in the main chamber is kept below the  $10^{-5}$  mbar range whereas it is kept at about  $10^{-4}$  mbar in the differentially-pumped tube when the HPLC pump is ON. Our equipment is an updated version of the equipment used in the reference.<sup>23</sup> The aqueous potassium chloride solution was prepared by mixing >99% KCl salt with deionized water. Filtering and degazing procedures were systematically performed before injecting the solution. The spectrometer resolution of about 0.6 eV was achieved with the 500 eV pass energy and 0.5 mm slits. The photon energy resolution achieved at 2.8 keV and 3.6 keV was about 0.3 eV and 0.4 eV, respectively.

The experimental 2D maps representing the dependence of the electron kinetic energy on the photon energy of KCl at the K-edges of  $\text{K}^+$  and  $\text{Cl}^-$ , are shown in Figs. 2 and 3, respectively.

### *Ab initio* calculations

The theoretical X-ray absorption spectra were computed for the hexa-coordinated clusters of both ions,  $\text{K}^+(\text{H}_2\text{O})_6$  and  $\text{Cl}^-(\text{H}_2\text{O})_6$ , which can be considered as representatives of the complete first solvation shell of the two ions<sup>24–26</sup>. The two structures were optimized at the DFT level of theory using the B3LYP functional and the 6-311++G(2d,2p) basis set<sup>27,28</sup>. The geometry optimization was performed with the Gaussian 09 package<sup>29</sup>. In order to obtain more realistic structures corresponding to the bulk solution, we carried out constrained geometry optimization starting with the equilibrium gas-phase geometries<sup>30</sup>(REF for Cl-) belonging to the  $D_3$  point group and increasing the angle  $\theta$  between the K-O/Cl-O bond and the  $C_3$  axis to  $55^\circ$  in the case of  $\text{K}^+$  and  $50^\circ$  in the case of  $\text{Cl}^-$ . This angle was chosen such that the O-K-O and O-Cl-O angles are around the maxima of the angular distributions obtained from quantum mechanics / molecular mechanics dynamical simulations in Ref.<sup>26</sup>. Moreover, we fixed the K-O and Cl-O distances to 2.840 Å and 3.140 Å, respectively, such that they correspond to the distances from other theoretical and experimental works<sup>24–26,31,32</sup>. The hexa-coordinated structures are presented in Fig. 4.

The energies and transition moments of the core excited states of the microsolvated clusters were computed with the algebraic diagrammatic construction method for the polarization propagator<sup>33</sup> within the core-valence separation approximation<sup>34–36</sup> (CVS-ADC(2)x) as implemented in the Q-Chem package<sup>37–40</sup>. In the case of  $\text{Cl}^-$  the 6-311++G(3df,3pd) basis set<sup>27,41</sup> (excluding the f functions) was used for all atoms, whereas in the case of  $\text{K}^+$  we used the 6-311+G(2d,p) basis set<sup>27,28</sup> on all atoms, and two additional sets of s, p and d diffuse functions were added on K. The use of a smaller basis set in the case of K is due to the higher number of atomic orbitals compared to the case of Cl, and therefore, prohibitively high cost of the CVS-ADC(2)x computation. In our calculations the core space comprises

the 1s orbital of  $\text{K}^+$  or  $\text{Cl}^-$ , whereas the remaining occupied orbitals are included in the valence space. For the calculations of the XAS spectra we used the  $\text{C}_2$  point group in the case of  $\text{K}^+(\text{H}_2\text{O})_6$  and  $\text{Cl}^-(\text{H}_2\text{O})_6$ . To account for the lifetime broadening due to the Auger decay of the core excited states, we convolved the theoretical spectra with a Lorentzian function of FWHM 0.74 eV and 0.62 eV in the case of  $\text{K}^+$  and  $\text{Cl}^-$ , respectively<sup>42</sup>. We analyzed the core excited states by expanding the singly occupied natural orbitals (SONOs)  $\psi_i$  of the microsolvated clusters in the basis of SONOs of the bare  $\text{K}^+$  or  $\text{Cl}^-$  ion  $\chi_{nl}$

$$\psi_i = \sum_{nl} a_{nl}^i \chi_{nl} \quad (1)$$

where  $n$  and  $l$  stand for the principal and orbital quantum numbers as described in Ref.<sup>18</sup>. The expansion coefficients  $a_{nl}^i$  show the degree of delocalization of the excited electron and the mixing of the core excited states in the crystal field created by the surrounding water molecules (see Fig. 4).

The final states following KLL resonant Auger decay of  $\text{K}^+(\text{H}_2\text{O})_6$  and  $\text{Cl}^-(\text{H}_2\text{O})_6$  were computed at the Configuration Interaction Singles (CIS) level using the Graphical Unitary Group Approach (GUGA) as implemented in the GAMESS-US package<sup>43–45</sup>. In order to account for the relaxation effects upon core ionization, we used a restricted open-shell Hartree-Fock reference wave function with a hole in the 2s orbital of both  $\text{K}^+$  and  $\text{Cl}^-$ . We used the 6-311++G(2d,2p) basis set<sup>27,28,41</sup> on all atoms. Additionally, the basis set was augmented with 2 sets of s, p, d diffuse functions in the case of  $\text{K}^+$ , and 3 sets of s, p, d diffuse functions in the case of  $\text{Cl}^-$ . The larger basis set employed in the case of Cl was necessary in order to ensure the convergence of the excited states. The active space comprises the 2s and 2p orbitals of K/Cl with occupancy fixed to 6 and all virtual orbitals with occupancy fixed to 1. The remaining doubly occupied orbitals were frozen in the calculation.<sup>46</sup>

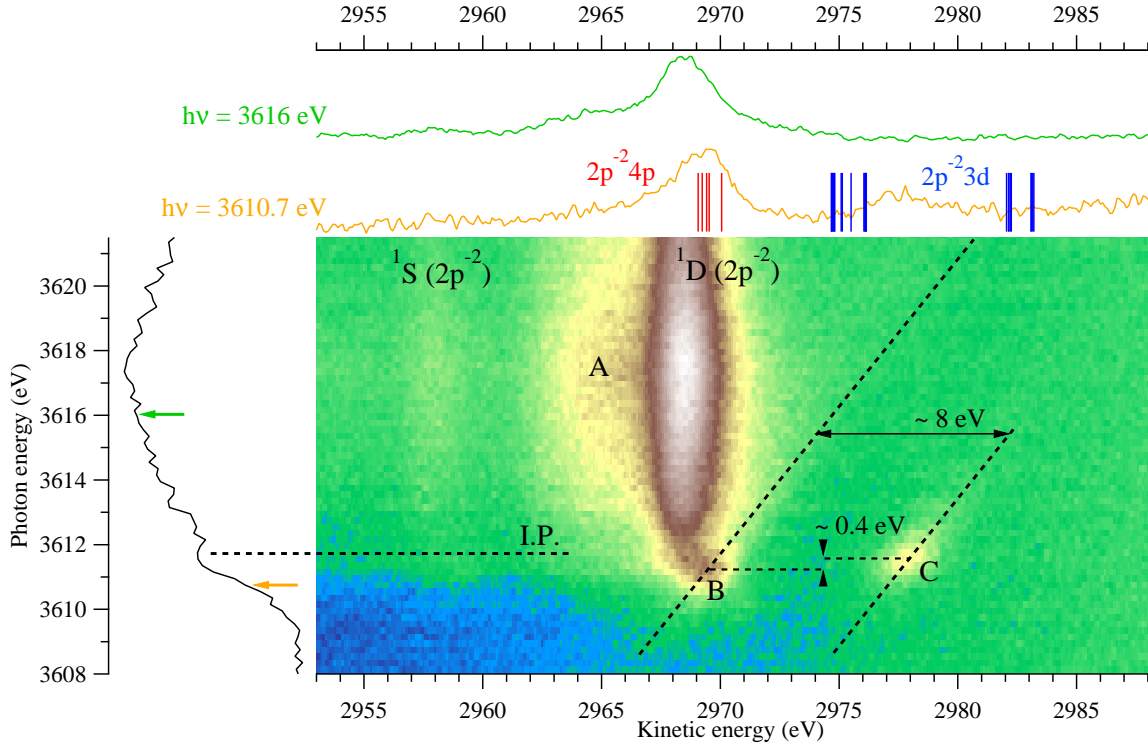


Figure 2: 2D map showing the kinetic energy of the electrons emitted in  $KL_{2,3}L_{2,3}$  Auger decay vs the photon energy in the vicinity of the K-edge of aqueous  $K^+$ . The black curve on the left represents the experimental partial electron yield spectrum of  $K^+$  obtained after integrating over the kinetic energies of the Auger electrons in the energy range presented on the figure. The upper panel shows two spectra at photon energies 3610.7 eV, and 3616 eV below and above the ionization potential at 3611.9 eV, respectively. The bars in the pre-edge cut correspond to the final  $2p^{-2} 3d$  (blue) and  $2p^{-2} 4p$  (red) doublet resonant Auger states of  $K^+(H_2O)_6$  computed at the CIS level (see Sec. for details). The features A, B and C are discussed in the text.



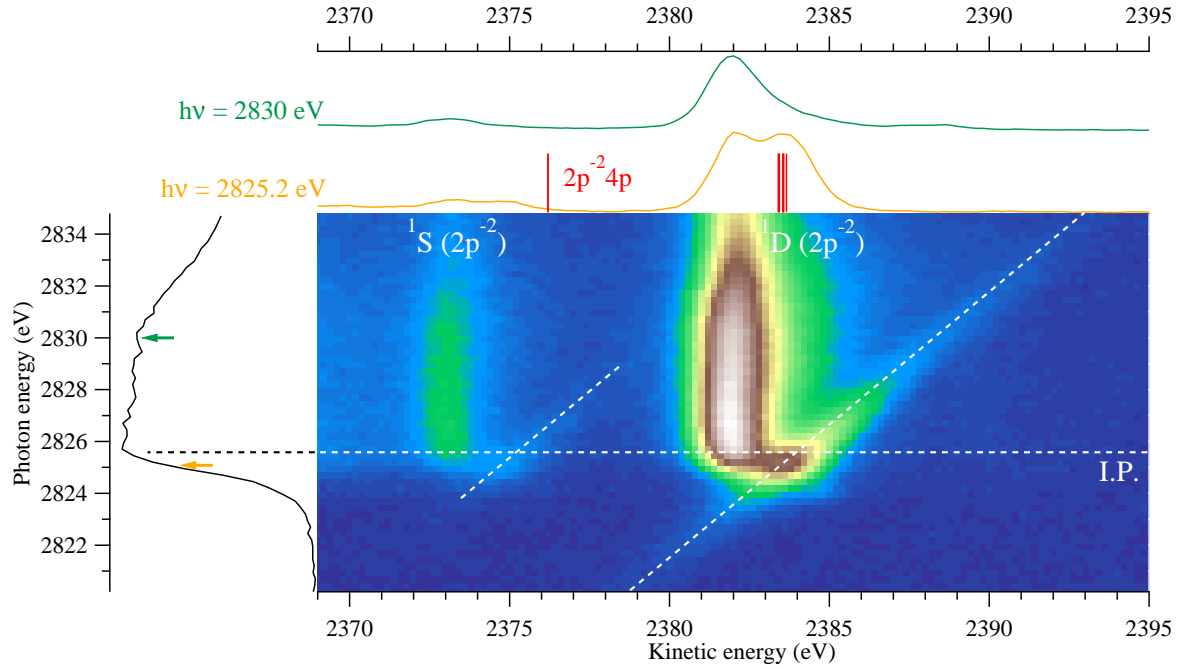
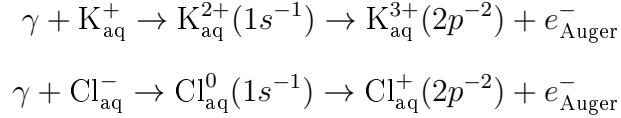


Figure 3: 2D map showing the kinetic energy of the electrons emitted in  $KL_{2,3}L_{2,3}$  Auger decay vs the photon energy in the vicinity of the K-edge of aqueous  $Cl^-$ . The black curve on the left represents the experimental partial electron yield spectrum of  $Cl^-$  obtained after integrating over the kinetic energies of the Auger electrons in the energy range presented on the figure. The upper panel shows two spectra at photon energies 2825.2 eV, and 2830.0 eV below and above the ionization potential at 2825.4 eV, respectively. The bars in the pre-edge cut correspond to the final  $2p^{-2} 3d$  (blue) and  $2p^{-2} 4p$  (red) doublet resonant Auger states of  $Cl^-(H_2O)_6$  computed at the CIS level (see Sec. for details).

# Results and discussion

## Normal Auger decay

The  $KL_{2,3}L_{2,3}$  normal Auger decay following K-shell ionization of aqueous  $K^+$  and  $Cl^-$  can be written as follows



It results in the population of  $2p^{-2}(^3P, ^1D, ^1S)$  final states. The  $^3P$  final states are expected to have a very low intensity since at the first order they are forbidden from parity conservation rules. In addition, in the photon energy range of interest, the tail of the  $^1D$  state described in the next paragraph, and the  $^1D\ 2p^{-2}V'$  dispersive state (see next section) overlap with the  $^3P$  state in the kinetic energy region where it is expected to occur, thus making it impossible to properly determine its position. In the case of  $K_{aq}^+$  the maxima of the  $^1S$  and  $^1D\ KL_{2,3}L_{2,3}$  Auger lines are located at 2958 eV and 2968.4 eV, respectively (see Fig. 2). For  $Cl_{aq}^-$ , the lines corresponding to the  $Cl^+(2p^{-2})\ ^1S$  and  $^1D$  states are located at 2373.2 eV and 2382.1 eV kinetic energy (see Fig. 3).

The  $KL_{2,3}L_{2,3}$  Auger lines do not disperse with photon energy except close to threshold due to the interaction between the photoelectron and Auger electron, i.e. the so-called post-collision interaction (PCI). As a result of this interaction, first, the peaks in the Auger spectrum become asymmetric with a shoulder at high kinetic energies, and second, they are shifted to higher kinetic energies close to threshold<sup>47,48</sup>. Consequently, one can attribute the high kinetic energy shoulder of the  $^1D$  and  $^1S$  peaks on Figs. 2 and 3 as resulting from PCI effect. The asymmetric tail of the peaks resulting from PCI can be clearly seen on the cuts taken at photon energies 3616 eV in the case of  $K^+$ , and 2830 eV in the case of  $Cl^-$ .

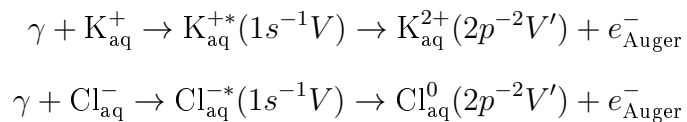
Further, we compare the positions of the normal KLL Auger lines of both  $Cl_{aq}^-$  and  $K_{aq}^+$

close to threshold with those recorded far from threshold, at photon energies  $h\nu = 5 \text{ keV}$  (see Ref.<sup>8</sup> for details). In this case, the maxima of the  $^1\text{D}$  and  $^1\text{S}$  states were found at lower values at 2381.1 eV and 2372.3 eV for  $\text{Cl}_{\text{aq}}^-$ , and 2967.4 eV and 2957 eV kinetic energy for  $\text{K}_{\text{aq}}^+$ , respectively. The lines observed at photon energies far from threshold and close to it appear thus to be shifted by  $\sim 1 \text{ eV}$ . The magnitude of the shift is the same for both ions suggesting that it does not depend on the initial charge of the ion, and it is almost constant in the photon energy range presented here. A possible explanation of the shift observed in our experiment is given in Ref.,<sup>49</sup> which focuses on the Auger decay of large Kr clusters on and just above the  $3d_{5/2}$  ionization threshold. The observed  $4d^4(^1\text{D})$  Auger peak was found to be shifted by 0.7 eV to higher kinetic energies compared to the position of the peak far above threshold. Moreover, the shift did not vary with the photon energy close to threshold. Consequently, it was proposed that this feature originates from a process of internal ionization, i.e. excitation of the photoelectron into the conduction band. Further investigations are, however, planned in the case of liquid samples.

Finally, the normal Auger  $^1\text{D}$  main line of  $\text{K}^+$  differs from that of  $\text{Cl}^-$  by the presence of a large shoulder (A on Fig. 2) on the low kinetic energy side at about 2965 eV kinetic energy. This shoulder is attributed to electron transfer from the water solvent molecules<sup>8</sup> to the 3d orbital of  $\text{K}^+$ . In the case of  $\text{Cl}^-$ , there is no experimental evidence of such intense electron transfer processes.

## Resonant Auger decay

The  $\text{KL}_{2,3}\text{L}_{2,3}$  Auger decay following resonant K-shell excitation of solvated  $\text{K}^+$  and  $\text{Cl}^-$  can be written as follows



where  $V$  and  $V'$  denote the unoccupied orbitals in the excited and singly ionized excited states, i. e. in the presence of the  $1s^{-1}$  and  $2p^{-2}$  core holes. The character of these states is discussed below.

**How are the IPs determined? 2D maps reveal the core excited states.** The pre-edge regions of the x-ray absorption spectra of  $K^+$  and  $Cl^-$  shown to the left on Figs. 2 and 3 do not exhibit any high intensity features due to the lifetime broadening and energetic proximity of the core excited states to the ionization threshold. Consequently, solely from these absorption spectra, one cannot conclude whether there are core excited states in the pre-edge structure, which can undergo resonant Auger decay. However, one can determine their excitation energies from the maxima of the resonant Auger features. Thus, for  $Cl^-$ , the lowest core excited state is located at 2825.2 eV, which agrees very well with the position of the  $Cl^- 1s \rightarrow 4p$  excitation determined from Cl K-edge XAS experiments in  $MgCl_2 \cdot 6H_2O$  and of  $SrCl_2/SrCl_2 \cdot 6H_2O$ <sup>50</sup> and  $MCl_4^-$  compounds<sup>51</sup>. In the case of  $K^+$ , there are two dispersive features with maxima at photon energies of 3611.2 eV (B) and 3611.6 eV (C), respectively (Fig. 2). The positions of these two core excited states are close to the energy of the  $1s \rightarrow 4p$  excitation in bare  $K^+$ , 3610.7 eV<sup>52</sup>.

The resonant Auger features produced in the decay of these core excited states appear to be quite different for  $Cl^-$  and  $K^+$ . In the spectrum of  $Cl^-$  shown in Fig. 3 there are two dispersive features on the high kinetic energy side of the main  $^1S$  and  $^1D$  lines, i.e. at 2825.2 eV photon energy and 2374.6 and 2383.4 eV kinetic energy. In the case of  $K^+$ , the  $^1S$  dispersive line cannot be clearly identified due to the presence of strong background. The dispersive feature close to the  $^1D$  main peak is observed (feature B) with a maximum located at  $h\nu = 3611.2$  eV and 2969.2 eV kinetic energy. An additional feature appears as a separate island away from the main lines on the 2D map of  $K^+$ . It is located at  $h\nu = 3611.6$  eV and 2978.1 eV kinetic energy (feature C), thus it is separated by approximately 400 meV photon energy and 8.3 eV kinetic energy from the feature B.

In order to rationalize the pre-edge region of the experimental XAS spectra and the

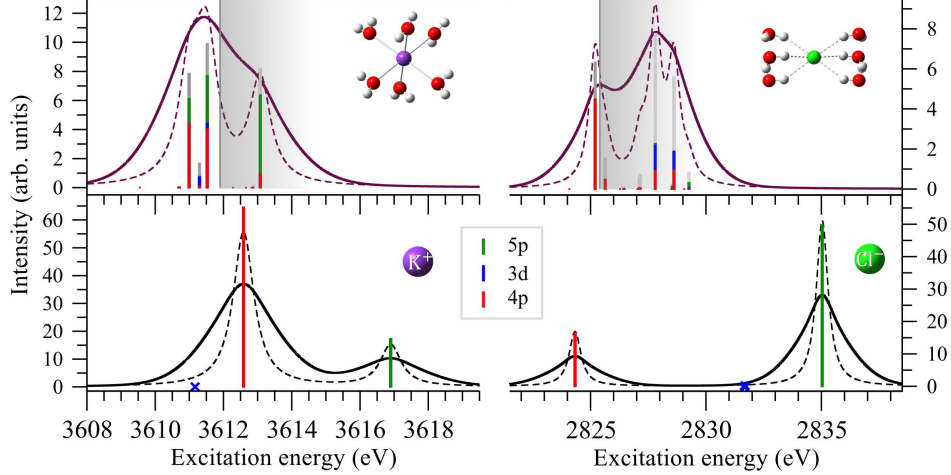


Figure 4: XAS spectra of the lowest K-shell transitions in the bare  $K^+$  (lower left panel) and  $Cl^-$  (lower right panel) ions and their 6-coordinated clusters (upper left panel,  $K^+(H_2O)_6$ , and upper right panel,  $Cl^-(H_2O)_6$ ). The theoretical stick spectra were convolved with a Lorentzian profile of FWHM 0.74 eV for  $K^+$  and 0.62 eV for  $Cl^-$  (dashed line) and a Voigt profile to account for the lifetime broadening and the experimental resolution (full line). The stick spectrum corresponds to the projections  $|a_{nl}^i|^2$  of the SONOs corresponding to the core excited states of the 6-coordinated clusters on the basis of SONOs corresponding to the  $1s \rightarrow 3d$ ,  $1s \rightarrow 4p$ , and  $1s \rightarrow 5p$  states in the bare  $K^+$  and  $Cl^-$  ions (Eq. 1). The theoretical XAS spectra of both  $K^+$  and  $Cl^-$  were shifted to higher photon energies such that the excitation energies of the lowest core excited states correspond to the experimentally determined energies – 3610.7 eV in the case of  $K^+$ , and 2825.2 eV in the case of  $Cl^-$ . The experimental ionization thresholds are depicted as grey boxes starting at photon energies of 3611.9 eV ( $K^+_{aq}$ ) and 2825.4 eV ( $Cl^-_{aq}$ ).

differences in the AES spectra of  $K^+_{aq}$  and  $Cl^-_{aq}$ , we computed the lowest core excited states of the bare  $K^+$  and  $Cl^-$  ions and their hexa-coordinated clusters. The theoretical XAS spectra are presented in Fig. 4. In the bare ions (lowermost panels on Fig. 4), the lowest energy peak corresponds to the dipole allowed  $1s \rightarrow 4p$  state. The next dipole allowed state,  $1s \rightarrow 5p$ , is located 4.3 eV and 10.8 eV higher in the cases of  $K^+$  and  $Cl^-$ , respectively. Together with the two dipole allowed transitions, we show the dipole forbidden  $1s \rightarrow 3d$  states of the bare ions as blue crosses at photon energies 3611.17 eV in the case of  $K^+$  and 2831.68 eV in the case of  $Cl^-$ , respectively. It is noteworthy that the positions of the  $1s \rightarrow 4p$  and  $1s \rightarrow 3d$  states are inverted in  $K^+$  and  $Cl^-$ . In the case of  $Cl^-$  the  $1s \rightarrow 4p$  excitation has lower energy and the  $1s \rightarrow 3d$  excitation is close to the  $1s \rightarrow 5p$  state. On the contrary, in  $K^+$  the  $1s \rightarrow 3d$  excitation has lower energy and lies below the  $1s \rightarrow 4p$  state. We note in

passing that the intensity of the  $\text{Cl}^-(1s \rightarrow 4p)$  state is lower than that of the  $\text{Cl}^-(1s \rightarrow 5p)$  state contrary to what is observed in  $\text{K}^+$ . This difference can be explained with the lower electron density of the 4p compared to the 5p electron in the region close to the core hole which thus results in the lower oscillator strength of the  $1s \rightarrow 4p$  compared to the  $1s \rightarrow 5p$  transition in  $\text{Cl}^-$  (see Fig. 1 in SI).

The water molecules in the first solvation shell have several effects on the core excited states. First, upon addition of water molecules, the degeneracy of the  $1s \rightarrow 4p$  state is lifted and the intensity of the resulting states in the cluster drops. Moreover, the character of these states changes – they are no longer of pure atomic character but they rather interact with states of the neighboring water molecules (shown as grey bars) and with other closely lying states of the bare ion, such as the dipole allowed  $1s \rightarrow 5p$  and dipole forbidden  $1s \rightarrow 3d$  state. Thus, the latter also acquire intensity in the cluster due to mixing with the dipole allowed states in the ligand field of the solvent. A similar effect was observed in the XAS spectra of microsolvated clusters of  $\text{Na}^+$  and  $\text{Mg}^{2+}$ <sup>18</sup>.

Further we assume that only the lowest peak in the theoretical XAS spectra is populated in the experiment for two reasons. First, due to the lifetime broadening, it spreads over approximately 2 eV which coincides with the width of the pre-edge structure in the experimental XAS spectra. Second, the splitting between the first core excited state and the ionization threshold in the experiment is 1.2 eV for  $\text{K}^+$  and 0.2 eV for  $\text{Cl}^-$ , and thus it is smaller than the splitting between the first and second peak in the theoretical spectra (1.5 eV for  $\text{K}^+$  and  $\sim 3$  eV for  $\text{Cl}^-$ , Fig. 4). In the 6-coordinated cluster (Fig. 4 upper left panel), which represents the complete first solvation shell around  $\text{K}^+$ , the lowest peak in the spectrum contains three states. The lowest and highest lying states are split by approximately 0.5 eV and they have mixed 4p and 5p character. The low intensity state in between these two states has a predominantly  $1s \rightarrow 3d$  character. Since the dispersive feature B appears at lower excitation energies compared to the feature C, we assume that it is produced in the resonant Auger decay of the lowest core excited states of  $\text{K}^+$ , which are predominantly of

$1s \rightarrow 4p$  character. Moreover, we can attribute the feature C to the resonant Auger decay of the low intensity dipole forbidden  $1s \rightarrow 3d$  state. Thus, we explain both the energy splitting of  $\sim 400$  meV photon energy of the two features, and the fact that island C has lower intensity than feature B.

In the hexa-coordinated cluster of  $\text{Cl}^-$ , the solvent molecules have little influence on the position and character of the first peak. Since there are no other ionic states close the  $1s \rightarrow 4p$  state in the bare ion, this state preserves its character in the cluster and interacts with states of the nearest water molecules. We attribute the two dispersive features on the 2D map of  $\text{Cl}^-$  and associated with the  $^1\text{S}$  and  $^1\text{D}$  terms, to the resonant Auger decay of these core excited states involving mostly the 4p orbitals of chloride.

To fully characterize the dispersive features on the experimental 2D maps, we also computed the lowest  $\text{K}^{2+}[2p^{-2}\text{nl}](\text{H}_2\text{O})_6$  and  $\text{Cl}^0[2p^{-2}\text{nl}](\text{H}_2\text{O})_6$  states of the hexa-coordinated clusters corresponding to the lowest final spectator resonant Auger states. They are shown as bars in the upper panels on the experimental resonant Auger spectra on Figs. 2 and 3. In both cases, we shifted the lowest  $2p^{-2}4p$  states such that they coincide with the maxima of the dispersive features on the high kinetic energy part of the  $^1\text{D}$  main line. Out of all final states we show only the doublets. Since the initial core excited states are populated by photon excitation, only doublet states are efficiently populated in the resonant Auger decay. The  $2p^{-2}\text{nl}$  states of  $\text{K}^+(\text{H}_2\text{O})_6$  and  $\text{Cl}^-(\text{H}_2\text{O})_6$  are substantially different and they reflect the fact that the 3d unoccupied orbitals of  $\text{K}^+$  are lower than the 4p orbitals, which is the opposite of what is observed in  $\text{Cl}^-$ .

As mentioned above, we attribute the island B to the decay of the lowest lying core excited state of the hexa-hydrated  $\text{K}^+$  cluster, which is of predominantly  $1s \rightarrow 4p$  character. Supposing that this state undergoes mostly pure spectator resonant Auger decay, which is the case of the  $1s \rightarrow 4p$  state in the isoelectronic Ar atom<sup>53</sup>, then the lowest states of  $2p^{-2}4p$  character located between 2969 and 2970.5 eV are populated. As can be seen from the Auger electron spectrum at  $h\nu = 3610.7$  eV (upper panel of Fig. 2), the lowest  $2p^{-2}4p$

states of  $\text{K}^+(\text{H}_2\text{O})_6$  starting at electron energy of 2969 eV are separated by  $\sim 5$  and 12-13 eV from the two groups of  $2\text{p}^{-2}3\text{d}$  states located at higher electron kinetic energies. Thus, the group of  $2\text{p}^{-2}3\text{d}$  states at  $\sim 2975$  eV lies closer to the position of island C. Consequently, we attribute this dispersive feature as originating from the resonant Auger decay of the  $1\text{s} \rightarrow 3\text{d}$  state of the 6-coordinated  $\text{K}^+$  cluster to the group of  $2\text{p}^{-2}3\text{d}$  states lying around 2975 eV. The splitting between the  $2\text{p}^{-2}4\text{p}$  and  $2\text{p}^{-2}3\text{d}$  states in our calculation is smaller than the splitting between the islands B and C. This difference may be due to the fact that we do not account for the effect of distant solvent shells in our calculation. Concerning the higher lying group of  $2\text{p}^{-2}3\text{d}$  states at kinetic energies between 2982 and 2983 eV, we conclude that these states are not populated via the Auger process since no additional experimental features are observed.

Another argument supporting the attribution of the island C as being of  $2\text{p}^{-2}3\text{d}$  character comes from the attribution of the A area as given in reference<sup>8</sup> and from the energy splitting between A and C. The A area originates from a charge transfer process between water (W) and core excited potassium and has the configuration  $\text{K}^{2+}(2\text{p}^{-2}3\text{d})\text{W}^{-1}$ . The ionization potential of water in the liquid phase is about 11 eV which fits well with the observed A-C splitting. Based only on these two simple energetic arguments we can attribute the C island to the a  $\text{K}^{2+}2\text{p}^{-2}3\text{d}$  configuration and note that neither  $2\text{p}^{-2}3\text{d}$  nor charge transfer states are present in the  $\text{Cl}^-$  case.

In the  $\text{Cl}^0[2\text{p}^{-2}\text{nl}](\text{H}_2\text{O})_6$  spectrum there are two groups of states split by about 7 eV (see upper panel of Fig. 3). The lower kinetic energy group corresponds to the  $2\text{p}^{-2}(^1\text{S})4\text{p}$  states, whereas the higher kinetic energy group corresponds to the  $2\text{p}^{-2}(^1\text{D})4\text{p}$  states. The splitting between the two groups is in good agreement with the experimental splitting between the dispersive features on the high kinetic energy sides of the  $^1\text{S}$  and  $^1\text{D}$  main peaks. Consequently, we attribute these dispersive features as resulting from the resonant Auger decay of the  $1\text{s} \rightarrow 4\text{p}$  core excited state of  $\text{Cl}^-_{\text{aq}}$  to the  $2\text{p}^{-2}(^1\text{S})4\text{p}$  and  $2\text{p}^{-2}(^1\text{D})4\text{p}$  final states. Similar dispersive features originating from the decay of the  $\text{Cl}(1\text{s} \rightarrow 4\text{p})$  state were



observed on the 2D map of chloromethane  $\text{CH}_3\text{Cl}$  recorded in the vicinity of the Cl K-edge in gas phase.<sup>54</sup> In this case, however, additional lower-lying core excited state are observed. They result from excitation to the LUMO of  $\text{CH}_3\text{Cl}$ , which is a linear combination of the C 2p and Cl 3p atomic orbitals. Since the 3p shell is fully occupied in  $\text{Cl}^-$ , such a core excited state is not observed in our experiment.

## Delocalization vs resonant Auger decay

As mentioned above, the delocalization of core excited electrons in aqueous solutions is ultrafast and as such it competes with the resonant Auger decay. In order to estimate the delocalization rate of the core excited electron at the pre-edges of  $\text{K}^+$  and  $\text{Cl}^-$ , we used the core-hole clock method as in the reference.<sup>55,56</sup>

In the case of  $\text{Cl}^-$ , and contrary to  $\text{K}^+$ , it was possible to perform the same data treatment as in Ref.,<sup>53</sup> i.e. for each photon energy step, all components of the 2D map shown in Fig. 3 were isolated by fitting procedures and their intensity integrated to get a partial electron yield as a function of the photon energy. The result is shown on Fig. 2 in the SI. The figure shows that there is a large overlap between the resonant and normal Auger contributions, due to the proximity of the resonance to the ionization potential and due to the very short lifetime of the corresponding states. At the specific photon energy corresponding to the lowest core excitation,  $h\nu = 2825.2\text{eV}$  (Fig. 3, upper panel) a double-peak structure is observed in the interval of kinetic energies  $2380 - 2385\text{eV}$ . The position of the first peak coincides with the main  $^1\text{D}$  line resulting from normal Auger, whereas the second peak at  $2383.5\text{eV}$  corresponds to the final resonant Auger states  $2\text{p}^{-2}(^1\text{D})4\text{p}$ . By fitting the peak with two Voigt functions, we determine the ratio of the intensities of these peaks to be  $\sim 1$ . Consequently, the delocalization time is of the same order as the Auger lifetime, i.e.  $\sim 1\text{fs}$ . The fast delocalization in this case is a result of the fact that the energy splitting between the  $\text{Cl}^-$  ( $1\text{s} \rightarrow 4\text{p}$ ) resonance and the ionization threshold is  $0.2\text{eV}$ , and thus, smaller than the lifetime broadening of  $0.62\text{eV}$ .

For potassium the treatment is more complex due to the presence of multiple simultaneous processes – normal, resonant Auger decay, charge transfer (CT) from solvent. To extract the intensity of each component from the 2D map shown in Fig. 2, one needs the spectral fingerprints of each process to be separated. However, as can be seen, this is not the case especially close to threshold in the kinetic energy region 2965 – 2970 eV. For instance at 3610.7 eV photon energy on the high-kinetic-energy side of the  $2p^{-2}(^1D)$  state, there are contributions from the PCI tail and from the dispersive  $2p^{-2}(^1D)4p$  state related to the B island. On the low-kinetic-energy side, the charge transfer process leads to a very large structure that unfortunately cannot be easily simulated by a known profile. However, the 1s core-hole lifetime is shorter for potassium than for chloride (0.9 vs. 1 fs) and moreover, the core excited state appears 1.2 eV below the ionization threshold whereas it is only 0.2 eV for chloride. Therefore, one can expect a much less efficient delocalization process compared to  $Cl^{-}_{aq}$ .

## Conclusion

Using a combination of x-ray absorption and Auger electron spectroscopy in the tender x-ray regime, in this work we studied the electronic structure of aqueous solution of KCl at the K-edges of both K and Cl. The Auger electron spectra of both ions as a function of photon energy exhibit features of normal as well as resonant Auger processes. To interpret the resonant Auger features in the experimental spectrum, we performed *ab initio* calculations on microsolvated clusters of  $K^{+}$  and  $Cl^{-}$ . Our calculations show that the energy ordering of the 3d and 4p virtual orbitals of  $Cl^{-}$  is inverted compared to  $K^{+}$ , and also that the energy splitting between the bright  $1s \rightarrow 4p$  and dark  $1s \rightarrow 3d$  core excited states is larger in the chlorine case. Thus, the energetic proximity of the 3d and 4p orbitals in the bare  $K^{+}$  ion results in the dipole forbidden  $1s \rightarrow 3d$  state acquiring intensity in a solution as a result of mixing with the dipole allowed  $1s \rightarrow 4p$  excitation. The spectator Auger decay of this state

produces an additional dispersive feature which is manifest as a separate island in the Auger electron spectrum at high kinetic energies. In the case of  $\text{Cl}^-$  the two core excited states do not interact, and therefore, only fingerprints of the population and Auger decay of the dipole allowed  $1s \rightarrow 4p$  state are observed in the spectrum. Moreover, using the core-hole clock method we estimated the time of delocalization of the core excited electron at the pre-edge region of  $\text{Cl}^-_{\text{aq}}$ . Our results show that in this case, the resonant Auger decay and the delocalization of the excited electron occur on a comparable timescale. In the case of  $\text{K}^+_{\text{aq}}$ , we cannot make an accurate estimate, however, one can expect a much less efficient delocalization of the core excited electron.

Our work shows that the combination of x-ray absorption and resonant Auger spectroscopies is a sensitive probe of the electronic structure of solvated ions. The reported results are an important first step in the study of the electronic decay processes following photoabsorption in the tender x-ray regime, and they can have implications in revealing the mechanisms of radiation damage in biologically relevant systems.

## Acknowledgement

We thank Prof. Nobuhiro Kosugi and Dr. Matjaž Žitnik for the fruitful discussions. Experiments were performed at the GALAXIES beamline, SOLEIL Synchrotron, France (Proposal No. 20140160). The authors are grateful to the SOLEIL staff for assistance during the beamtime. This project has received funding from the Research Executive Agency (REA) under the European Union's Horizon 2020 research and innovation programme Grant agreement No 705515. Campus France and the PHC SIAM exchange program are acknowledged for financial support.

## Supporting Information Available

- suppinfo.pdf: contains the radial density distributions of the core excited states of the bare ions.

## References

- (1) Smith, J. W.; Saykally, R. J. *Chem. Rev.* **2017**, *117*, 13909–13934, PMID: 29125751.
- (2) O’Neill, P.; Stevens, D. L.; Garman, E. F. *J. Synchrotron Radiat.* **2002**, *9*, 329–332.
- (3) Carugo, O.; Carugo, K. D. *Trends Biochem. Sci.* **2005**, *30*, 213–219.
- (4) Stumpf, V.; Gokhberg, K.; Cederbaum, L. S. *Nat. Chem.* **2016**, *8*, 237–241.
- (5) Pokapanich, W.; Bergersen, H.; Bradeanu, I. L.; Marinho, R. R. T.; Lindblad, A.; Legendre, S.; Rosso, A.; Svensson, S.; Björneholm, O.; Tchapyguine, M.; Öhrwall, G.; Kryzhevoi, N. V.; Cederbaum, L. S. *J. Am. Chem. Soc.* **2009**, *131*, 7264–7271.
- (6) Pokapanich, W.; Kryzhevoi, N. V.; Ottosson, N.; Svensson, S.; Cederbaum, L. S.; Öhrwall, G.; Björneholm, O. *J. Am. Chem. Soc.* **2011**, *133*, 13430.
- (7) Unger, I.; Seidel, R.; Thürmer, S.; Pohl, M. N.; Aziz, E. F.; Cederbaum, L. S.; Muchová, E.; Slavíček, P.; Winter, B.; V., K. N. *Nat. Chem.* **2017**, *9*, 708.
- (8) Céolin, D.; Kryzhevoi, N. V.; Nicolas, C.; Pokapanich, W.; Choksakulporn, S.; Songsiriritthigul, P.; Saisopa, T.; Rattanachai, Y.; Utsumi, Y.; Palaudoux, J.; Öhrwall, G.; Rueff, J.-P. *Phys. Rev. Lett.* **2017**, *119*, 263003.
- (9) Stoychev, S. D.; Kuleff, A. I.; Tarantelli, F.; Cederbaum, L. S. *J. Chem. Phys.* **2008**, *129*, 074307.
- (10) Demekhin, P. V.; Scheit, S.; Stoychev, S. D.; Cederbaum, L. S. *Phys. Rev. A* **2008**, *78*, 043421.

- (11) Demekhin, P. V.; Chiang, Y.-C.; Stoychev, S. D.; Kolorenč, P.; Scheit, S.; Kuleff, A. I.; Tarantelli, F.; Cederbaum, L. S. *J. Chem. Phys.* **2009**, *131*, 104303.
- (12) Ouchi, T.; Sakai, K.; Fukuzawa, H.; Higuchi, I.; Demekhin, P. V.; Chiang, Y.-C.; Stoychev, S. D.; Kuleff, A. I.; Mazza, T.; Schöffler, M.; Nagaya, K.; Yao, M.; Tamenori, Y.; Saito, N.; Ueda, K. *Phys. Rev. A* **2011**, *83*, 053415.
- (13) Miteva, T.; Chiang, Y.-C.; Kolorenč, P.; Kuleff, A. I.; Cederbaum, L. S.; Gokhberg, K. *J. Chem. Phys.* **2014**, *141*, 164303.
- (14) Travnikova, O.; Marchenko, T.; Goldsztejn, G.; Jänkälä, K.; Sisourat, N.; Carniato, S.; Guillemin, R.; Journal, L.; Céolin, D.; Püttner, R.; Iwayama, H.; Shigemasa, E.; Pincastelli, M. N.; Simon, M. *Phys. Rev. Lett.* **2016**, *116*, 213001.
- (15) Gokhberg, K.; Kolorenč, P.; Kuleff, A. I.; Cederbaum, L. S. *Nature* **2014**, *505*, 661–663.
- (16) Trinter, F. et al. *Nature* **2014**, *505*, 664–666.
- (17) Björneholm, O.; Federmann, F.; Fössing, F.; Möller, T. *Phys. Rev. Lett.* **1995**, *74*, 3017–3020.
- (18) Miteva, T.; Wenzel, J.; Klaiman, S.; Dreuw, A.; Gokhberg, K. *Phys. Chem. Chem. Phys.* **2016**, *18*, 16671–16681.
- (19) Nordlund, D.; Ogasawara, H.; Bluhm, H.; Takahashi, O.; Odelius, M.; Nagasono, M.; Pettersson, L. G. M.; Nilsson, A. *Phys. Rev. Lett.* **2007**, *99*, 217406.
- (20) Ottosson, N.; Odelius, M.; Spångberg, D.; Pokapanich, W.; Svanqvist, M.; Öhrwall, G.; Winter, B.; Björneholm, O. *J. Am. Chem. Soc.* **2011**, *133*, 13489–13495.
- (21) Céolin, D.; Ablett, J.; Prieur, D.; Moreno, T.; Rueff, J.-P.; Marchenko, T.; Journal, L.; Guillemin, R.; Pilette, B.; Marin, T.; Simon, M. *J. Electron Spectrosc. Relat. Phenom.* **2013**, *190*, Part B, 188 – 192.

- (22) Rueff, J.-P.; Ablett, J. M.; Céolin, D.; Prieur, D.; Moreno, T.; Balédent, V.; Lassalle-Kaiser, B.; Rault, J. E.; Simon, M.; Shukla, A. *J. Synchrotron Rad.* **2015**, *22*, 175–179.
- (23) Faubel, M.; Schlemmer, S.; Toennies, J. P. *Z. Phys. D* **1988**, *10*, 269–277.
- (24) Ohtaki, H.; Radnai, T. *Chem. Rev.* **1993**, *93*, 1157–1204.
- (25) Soper, A. K.; Weckström, K. *Biophys. Chem.* **2006**, *124*, 180 – 191.
- (26) Ma, H. *Int. J. Quant. Chem.* **2014**, *114*, 1006–1011.
- (27) Krishnan, R.; Binkley, J. S.; Seeger, R.; Pople, J. A. *J. Chem. Phys.* **1980**, *72*, 650–654.
- (28) Blaudeau, J.-P.; McGrath, M. P.; Curtiss, L. A.; Radom, L. *J. Chem. Phys.* **1997**, *107*, 5016–5021.
- (29) Frisch, M. J. et al. Gaussian 09 Revision D.01. Gaussian Inc. Wallingford CT 2009.
- (30) Lee, H. M.; Kim, J.; Lee, S.; Mhin, B. J.; Kim, K. S. *J. Chem. Phys.* **1999**, *111*, 3995–4004.
- (31) Ge, L.; Bernasconi, L.; Hunt, P. *Phys. Chem. Chem. Phys.* **2013**, *15*, 13169–13183.
- (32) Gora, R. W.; Roszak, S.; Leszczynski, J. *Chem. Phys. Lett.* **2000**, *325*, 7 – 14.
- (33) Schirmer, J. *Phys. Rev. A* **1982**, *26*, 2395–2416.
- (34) Barth, A.; Schirmer, J. *J. Phys. B At. Mol. Opt. Phys.* **1985**, *18*, 867.
- (35) Cederbaum, L. S.; Domcke, W.; Schirmer, J. *Phys. Rev. A* **1980**, *22*, 206–222.
- (36) Barth, A.; Cederbaum, L. S. *Phys. Rev. A* **1981**, *23*, 1038–1061.
- (37) Wenzel, J.; Wormit, M.; Dreuw, A. *J. Comp. Chem.* **2014**, *35*, 1900–1915.
- (38) Wenzel, J.; Wormit, M.; Dreuw, A. *J. Chem. Theory Comput.* **2014**, *10*, 4583–4598.

- (39) Wormit, M.; Rehn, D. R.; Harbach, P. H.; Wenzel, J.; Krauter, C. M.; Epifanovsky, E.; Dreuw, A. *Mol. Phys.* **2014**, *112*, 774–784.
- (40) Shao, Y. et al. *Mol. Phys.* **2015**, *113*, 184–215.
- (41) McLean, A. D.; Chandler, G. S. *J. Chem. Phys.* **1980**, *72*, 5639–5648.
- (42) Krause, M. O.; Oliver, J. H. *J. Phys. Chem. Ref. Data* **1979**, *8*, 329–338.
- (43) Brooks, B. R.; Laidig, W. D.; Saxe, P.; Handy, N. C.; Schaefer III, H. F. *Phys. Scr.* **1980**, *21*, 312.
- (44) Brooks, B. R.; Schaefer, H. F. *J. Chem. Phys.* **1979**, *70*, 5092–5106.
- (45) Schmidt, M. W.; Baldridge, K. K.; Boatz, J. A.; Elbert, S. T.; Gordon, M. S.; Jensen, J. H.; Koseki, S.; Matsunaga, N.; Nguyen, K. A.; Su, S.; Windus, T. L.; Dupuis, M.; Montgomery, J. A. *J. Comp. Chem.* **1993**, *14*, 1347–1363.
- (46) Mosnier, J.-P.; Kennedy, E. T.; van Kampen, P.; Cubaynes, D.; Guilbaud, S.; Sisourat, N.; Puglisi, A.; Carniato, S.; Bizau, J.-M. *Phys. Rev. A* **2016**, *93*, 061401.
- (47) Russek, A.; Mehlhorn, W. *J. Phys. B At. Mol. Opt. Phys.* **1986**, *19*, 911.
- (48) Guillemin, R.; Sheinerman, S.; Püttner, R.; Marchenko, T.; Goldsztejn, G.; Journal, L.; Kushawaha, R. K.; Céolin, D.; Piancastelli, M. N.; Simon, M. *Phys. Rev. A* **2015**, *92*, 012503.
- (49) Tchapyguine, M.; Kivimäki, A.; Peredkov, S.; Sorensen, S. L.; Öhrwall, G.; Schulz, J.; Lundwall, M.; Rander, T.; Lindblad, A.; Rosso, A.; Svensson, S.; Mårtensson, N.; Björneholm, O. *J. Chem. Phys.* **2007**, *127*, 124314.
- (50) Sugiura, C. *J. Chem. Phys.* **1982**, *77*, 681–682.
- (51) Shadle, S. E.; Hedman, B.; Hodgson, K. O.; Solomon, E. I. *J. Am. Chem. Soc.* **1995**, *117*, 2259–2272.

- (52) Hertlein, M. P.; Adaniya, H.; Amini, J.; Bressler, C.; Feinberg, B.; Kaiser, M.; Neumann, N.; Prior, M. H.; Belkacem, A. *Phys. Rev. A* **2006**, *73*, 062715.
- (53) Céolin, D.; Marchenko, T.; Guillemin, R.; Journal, L.; Kushawaha, R. K.; Carniato, S.; Huttula, S.-M.; Rueff, J. P.; Armen, G. B.; Piancastelli, M. N.; Simon, M. *Phys. Rev. A* **2015**, *91*, 022502.
- (54) Goldsztejn, G.; Marchenko, T.; Püttner, R.; Journal, L.; Guillemin, R.; Carniato, S.; Selles, P.; Travnikova, O.; Céolin, D.; Lago, A. F.; Feifel, R.; Lablanquie, P.; Piancastelli, M. N.; Penent, F.; Simon, M. *Phys. Rev. Lett.* **2016**, *117*, 133001.
- (55) Björneholm, O.; Nilsson, A.; Sandell, A.; Hernnäs, B.; Mrtensson, N. *Phys. Rev. Lett.* **1992**, *68*, 1892–1895.
- (56) Karis, O.; Nilsson, A.; Weinelt, M.; Wiell, T.; Puglia, C.; Wassdahl, N.; Mårtensson, N.; Samant, M.; Stöhr, J. *Phys. Rev. Lett.* **1996**, *76*, 1380–1383.



# Graphical TOC Entry

